Faraday Discussions

Accepted Manuscript

This manuscript will be presented and discussed at a forthcoming Faraday Discussion meeting. All delegates can contribute to the discussion which will be included in the final volume.

Register now to attend! Full details of all upcoming meetings: http://rsc.li/fd-upcoming-meetings

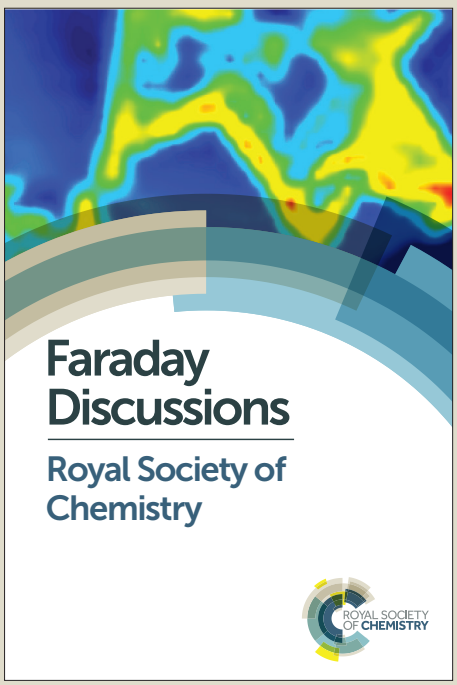

This is an *Accepted Manuscript*, which has been through the Royal Society of Chemistry peer review process and has been accepted for publication.

Accepted Manuscripts are published online shortly after acceptance, before technical editing, formatting and proof reading. Using this free service, authors can make their results available to the community, in citable form, before we publish the edited article. We will replace this *Accepted Manuscript* with the edited and formatted *Advance Article* as soon as it is available.

You can find more information about *Accepted Manuscripts* in the Information for Authors.

Please note that technical editing may introduce minor changes to the text and/or graphics, which may alter content. The journal's standard Terms & Conditions and the Ethical guidelines still apply. In no event shall the Royal Society of Chemistry be held responsible for any errors or omissions in this *Accepted Manuscript* or any consequences arising from the use of any information it contains.

ROYAL SOCIETY OF CHEMISTRY

www.rsc.org/faraday_d

CREATED USING THE RSC REPORT TEMPLATE (VER. 3.1) - SEE WWW.RSC.ORG/ELECTRONICFILES FOR DETAILS
REVIEW Faraday Discussions www.rsc.org/xxxxxx | XXXXXXXX

Oxygen Reduction Reaction in Electrochemically Reduced Graphene Oxide

Santosh Kumar Bikkarolla[1], Peter Cumpson[2], Paul Joseph[3] and Papakonstantinou Pagona[1]*

We show that partially reduced graphene oxide electrocatalyst, synthesized by electrochemical reduction of graphene oxide (GO) displays significantly enhanced catalytic activity towards oxygen reduction reaction (ORR) in alkaline solutions compared to the starting GO. The electrochemical partial reduction of GO was confirmed by X-ray diffraction and X-ray photoelectron spectroscopy. Electrochemical impedance spectroscopy (EIS) verified the enhanced electron transfer ability of the electrochemically reduced graphene oxide (ErGO) compared to GO. The resultant ErGO electrode showed an enhanced capacitance and an ORR onset potential of -0.11 V vs Ag/AgCl similar to that of nitrogen doped reduced graphene oxide (NrGO) electrode produced by a hydrothermal process. However the ErGO exhibited considerably lower electron transfer numbers (2.0 – 3.3 at potential range of -0.4 V to -1.0 V) indicating that although both catalysts operate under combined $4e^-$ and $2e^-$ ORR processes, ErGO follows a more predominant $2e^-$ pathway. The ORR process in ErGO has been linked to the presence of quinone functional groups, which favour the $2e^-$ ORR pathway.

DOI: 10.1039/b000000x [DO NOT ALTER/DELETE THIS TEXT]

Introduction

The oxygen reduction reaction (ORR), which generates electricity through the electrochemical reduction of oxygen, underpins many clean-energy technologies such as fuel cells and metal-air batteries. However, progress is hampered by the large intrinsic overpotentials of the ORR on the cathode side of fuel cells demanding relatively high loading of platinum electrocatalysts, which is both expensive and scarce.[1] As a result, the development of inexpensive, stable and catalytically active materials for the ORR that can approach and ideally surpass the performance of Pt based catalysts is of great technological significance.

Recently, there has been an explosion of studies on introducing various heteroatoms (e.g. N, B, P, S, and I)[2-12] or a combination of those[13-15] into carbon nanomaterials demonstrating a competitive ORR activity in alkaline electrolytes compared to the benchmark Pt/C catalyst. The phenomenon has been elucidated using density functional calculations, where it was found that the heteroatoms induce an uneven charge distribution in the adjacent sites, which alters the local spin or charge density thus promoting O_2 adsorption and facilitating molecular oxygen activation and subsequent O=O bond breaking.[16, 17]

Since the discovery of graphene, immense efforts have been focused on GO, because it is the most promising precursor for obtaining large quantities of this unique material. Graphene oxide can be visualized as individual sheets of graphene

decorated with oxygen functional groups on both basal planes and edges, which has been prepared by oxidative exfoliation of graphite. GO needs to be reduced to graphene with thermal or chemical reduction to recover its conducting properties. Thermal treatment at 1000 ^{0}C[18] or chemical reduction with hydrazine,[19] sodium borohydride,[20] aluminium hydride,[21] ammonium hydroxide and hydrothermal treatment with hydrazine[22] and ammonium thiocynate[23] can partially remove the oxygen functionalities on the basal plane and edges of the graphene oxide sheets. In the reduction process the sp^2 carbon network is restored, which improves the electrical conductivity of the material. These methods are suitable for the production of large scale quantities of reduced graphene oxide, however the majority of those necessitate the use of high temperatures and environmentally non-friendly reducing agents. In contrast, electrochemical reduction of GO doesn't require the use of any hazardous chemical reducing agents or high temperatures and the process is fast and simple.[24-34]

ErGO has shown promising characteristics for applications in supercapacitors,[30, 31, 35-37] biosensors,[26, 34, 38-40] due to its high surface area, presence of functional groups and increased conductivity. However the ORR performance of ErGO has not been investigated systematically. The work by D. Huang et al[29] was centred on the ORR study of electrochemically reduced layer-by-layer (LBL) self-assembly of negatively charged GO and positively charged PDDA rather than the ORR study of electrochemically reduced GO itself. The ORR performance of ErGO in alkaline (0.1 M KOH) solutions is only mentioned peripherally[29]. Y. Shao et al[33] reported the ORR performance of ErGO in acidic media (0.5 M H_2SO_4) in the form of a cyclic voltamogram, with no detailed kinetic or mechanistic studies.

In this work ErGO is synthesised by reducing the graphene oxide through repetitive cathodic cycling in the potential range 0 to -1.5 V in N_2 saturated 0.1 M Na_2SO_4 solution.[41, 42] The material is further explored as metal free catalyst for ORR applications in alkaline solutions by carrying out kinetic studies, and evaluating its electrochemically active surface area and methanol tolerance. In addition the ORR performance of ErGO is compared to that of nitrogen doped reduced graphene oxide (NrGO) prepared by a hydrothermal route.

Experimental section

Synthesis of NrGO

Graphite oxide was prepared by modified Hummer's method. GO was exfoliated in water by ultrasonication for 2 hrs. GO dispersion was centrifuged at 1000 rpm for 5 min to remove any thicker graphite oxide and the supernatant was centrifuged at 3000 rpm for 30 min. The obtained graphene oxide pellet was dried in oven at 60 ^{o}C for 48 hrs. NrGO was synthesized through hydrothermal reaction of graphene oxide with ammonia and hydrazine. In a typical experiment as synthesized graphite oxide was suspended in water to give a concentration of 1 mg/ml followed by sonication of 2 hrs. 70 ml of above solution pH was adjusted to 10 by ammonia hydroxide and 1 ml of hydrazine (35 wt% in H_2O) was added to the solution and stirred for 15 min. The solution was transferred to 100 ml teflon lined vessel to carry out the hydrothermal reaction at 160^{o}C for three hours. The resultant product was cleaned

with plenty of DI (deionized) water and collected by centrifugation at 3000 rpm for 45 min. The pellet was dried under vacuum at 60°C for 48 hrs.

Electrochemical reduction of GO

A total of 5 mg of graphite oxide was ultrasonicated in 1 ml of DI water for 60 min. To the homogenously dispersed GO solution 50 µl of Nafion was added and further sonicated for 30 min. The GO solution (4 µl) was applied onto 3 mm glassy carbon electrode (GCE) and dried under infrared lamp. The electrochemical reduction was carried out with cyclic voltammetry in the potential range 0 to -1.5 V vs. Ag/AgCl at a scan rate of 50 mV/sec in N_2 saturated 0.1 M Na_2SO_4 solution in a standard three electrode cell with Ag/AgCl as reference electrode and platinum as counter electrode. CVs in N_2 saturated 0.1 M Na_2SO_4 is shown in Figure S3.

Electrochemical Measurements

The Oxygen reduction reactions were carried out in 0.1 M KOH solution. The electrolyte was saturated with O_2 by bubbling O_2 for 15 min. A flow of O_2 was maintained over the electrolyte during the measurements. Cyclic voltammograms were collected at a scan rate 0.1 V/sec after atleast 25 times cycling of the electrode at 0.1 V/sec. RDE measurements were collected at a scan rate of 10 mV/sec. Kinetic analysis was performed using the Koutecky-Levich equation given below.

$$\frac{1}{J} = \frac{1}{J_L} + \frac{1}{J_K} = \frac{1}{nFkC_0} + \frac{1}{0.62nFD^{\frac{2}{3}}\vartheta^{-\frac{1}{6}}C_0\omega^{\frac{1}{2}}} \dots\dots\dots\dots (1)$$

Where J is the measured current density, J_K and J_L are kinetic and limiting diffusion current densities. n is the electron transfer number in the ORR process. F is the Faraday constant (96500 C/mol), C_0 is the bulk concentration of O_2 (1.2 x 10^{-6} mol/cm^3), D is the diffusion constant of O_2 in 0.1 M KOH (1.9 x 10^{-5} cm^2/sec), ν is the kinematic viscosity of the electrolyte (0.01 cm^2/sec) and ω is the angular frequency of the disk (2πN, N is the linear frequency) and k is electron transfer rate constant.

Structural characterization

X-ray photoelectron spectroscopy was carried on a Kratos Axis Nova XPS equipped with A1 Kα (hν = 1486.6 eV) X-ray source at NEXUS laboratory. X-ray diffraction (XRD) analysis was performed on a Bruker D8-discover diffractometer fitted with global mirror (Cu Kα radiation source λ = 1.540 Å). Scanning electron microscopy images were obtained on FEI quanta 200 3D at 20 kV accelerating voltage. High resolution Transmission electron microscopy (HRTEM) images were obtained on Jeol JEM 2011. Raman spectroscopy was done with ISA Lab ram equipped with 633 nm laser.

For XPS measurements GO without nafion was drop dried on gold coated substrate and reduced in the potential range 0 to -1.2 V vs Ag/AgCl for 22 CVs. For all the remaining structural characterization nafion was present in the GO solution

and the measurements were taken on GCE. The TEM samples were prepared by carefully removing the material from the GCE, followed by ultrasonication in isopropanol and coating the TEM grids with few microliters. For XRD measurements the ErGO was scraped off from GCE, followed by sonication in 70% ethanol and was drop dried on silicon substrate. SEM imaging carried out on GCE electrode.

Results and discussion

XPS was used to determine the elemental composition and bonding states of GO, ErGO (GO reduced for 22CVs) and NrGO. Figure 1(a-c) shows the C 1s of GO, ErGO and NrGO. The high resolution C 1s of GO shows two well defined peaks which is a signature of extreme oxidation of GO. C1s core level spectra for GO and ErGO samples contain four major peaks at 284.4 eV, 285.1 eV, 286.46 eV and 287.9 eV which are attributed to the sp^2 carbon, hydroxyl (C-OH), epoxide (C-O-C) groups, and the combined contribution from carbonyl (>C=O) and carboxyl (HO-C=O) groups[18, 43, 44] . The C 1s of NrGO can be fitted into three components at 284.4 eV, 285.1 eV and 287.7 eV which correspond to sp^2 carbon, C-N and a contribution from carbonyl and carboxylic groups.[45]

Figure 1 (d-e) shows the O 1s spectra of GO, ErGO. Deconvolution of O1s spectra produces 3 main peaks around 531.20, 532.2 and 533.3 eV assigned to C= O (Oxygen doubly bonded to aromatic Carbon-denoted as I1), C-O (Oxygen singly bonded to aliphatic Carbon- denoted as I2), and Phenolic (Oxygen singly bonded to aromatic Carbon- denoted as I3) groups respectively. Formation of quinone groups on ErGO is clearly evidenced from the broadening of the O1s peak at the low energy region. Figure 1 (f) shows the N1s of NrGO. The N 1s in NrGO can be divided into four components pyridinic N (398.8 eV), pyrrolic N (400.0 eV) graphitic N (401.54 eV) and pyridine N-oxide (403.4 eV) these assignments are in agreement with the literature.[22]

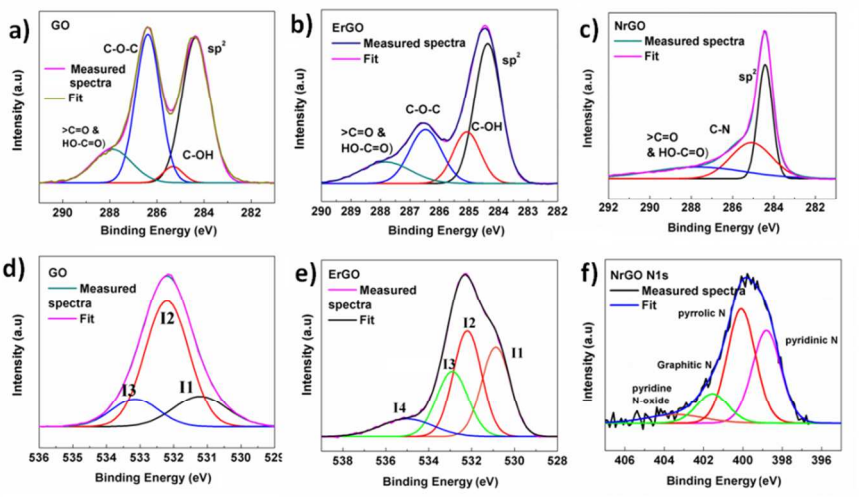

Fig.1: (a-c) shows the high resolution C 1s XPS spectra of GO, ErGO and NrGO. (d-e) shows the high resolution O 1s XPS spectra of GO, ErGO. (f) Shows the high resolution N 1s XPS spectra of NrGO.

The C/O ratios in the case of GO, ErGO and NrGO are 2.5, 4.0 and 9.6 respectively. The high content of the oxygen in the reduced sample could be due to the following reason. Due to the limited number of cycles employed here (22 cycles) for preparing the sample for XPS measurements, reduction may take place only on the first few surface layers, whereas the XPS is able to probe the underneath highly oxidised layers (XPS probing length can be as high as 10 nm).[25, 33]

It is worth mentioning that wide XPS spectra of ErGO revealed the presence of Na and S elements, which were originated from the Na_2SO_4 electrolyte used for the reduction process (see Fig S1). Similar impurities were also present in reported work of electrochemical reduction of GO over extended number of cycles.[33] In our case reducing the GO for higher number of cycles didn't improve ORR performance as discussed later. Although the presence of sulphur in carbon related materials has been claimed to act as an active site for ORR, here its presence is in minute amounts compared to those of oxygen.

Figure 2a shows the powder XRD spectra of GO, ErGO/nafion and NrGO. The GO spectrum shows a characteristic peak at 11.9°. After electrochemical reduction of GO there are four characteristic peaks 11.9°, 17.5°, 24° 38.5 ° and 44°.The peaks at 24° and 44° correspond to (002) and (001) planes of graphitic carbon. The peak at 38.5° corresponds to Na_2SO_4 (Figure S6). The low intensity of the (002) peak reveals that only the top surface of GO is reduced, which confirms that the electrochemical reduction is active only for the few surface layers. The peak at 17.5° corresponds to nafion, which helps in binding the graphene oxide to the GCE. The XRD pattern of NrGO shows two distinctive peaks at 24.5° and 43.0° corresponding to the (002) and (100) reflections of graphitic carbon. The average interlayer distance was calculated as 3.62 Å which is greater than the graphite interlayer distance of 3.33 Å which indicates a moderate oxidation level present in the NrGO.

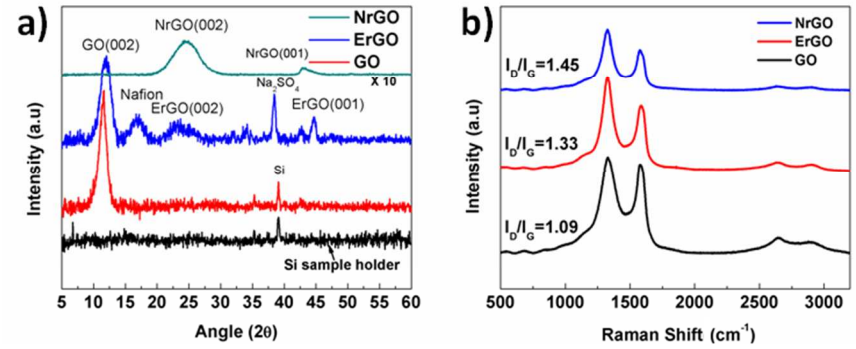

Fig. 2: (a) Shows the XRD spectra of GO and ErGO. (b) Raman spectra of GO and ErGO.

Raman spectroscopy is an important tool in characterising carbon materials because it is able to provide information on crystalline size, degree of disorder and

distinguish between single layer graphene from multilayer graphene. G and D band of carbon materials are assigned to the E_{2g} phonon mode of sp^2 carbon atoms and the breathing mode of κ-point phonons of A_{1g} symmetry. Figure 2b shows the Raman spectra of GO, ErGO and NrGO. The raman spectra of GO shows two bands at 1324 cm^{-1} and 1579 cm^{-1} with I_D/I_G ratio of 1.09. After electrochemical and hydrothermal reduction of GO the I_D/I_G ratio is increased to 1.33 and 1.45 indicating a decrease in the size of the sp^2 domain and restoration of sp^2 network upon electrochemical reduction of GO.[18, 43, 46]

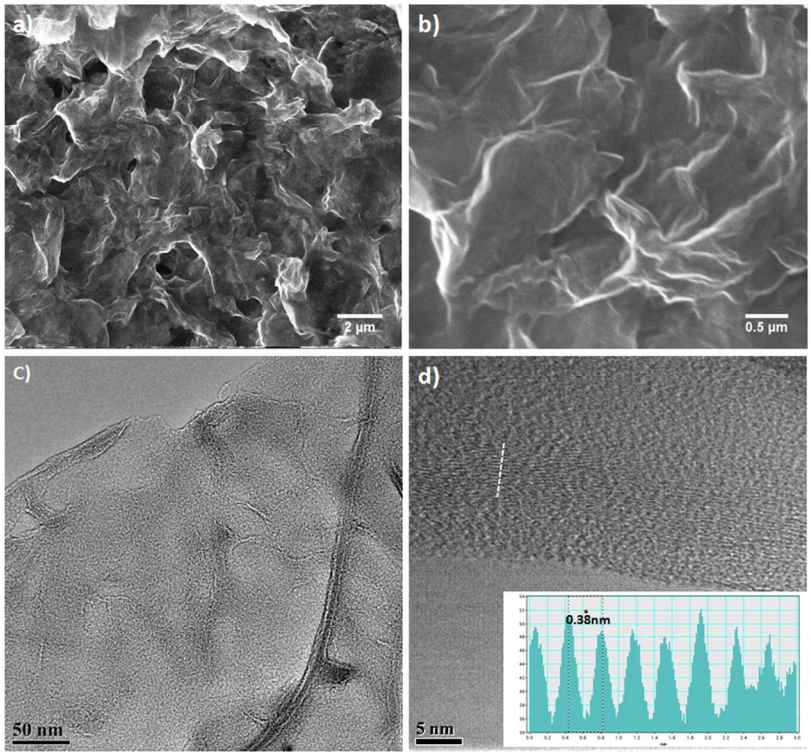

Fig. 3: (a-b) SEM images of ErGO on GCE. (c) Shows the TEM image of ErGO. (d) Shows the HRTEM image of ErGO and inset shows the distance between successive layers of ErGO.

Figure 3a and 3b shows SEM images of ErGO. These images indicate that the ErGO has a 3D porous morphology similar to that of reduced GO sheets derived from hydrothermal reduction. Further information on ErGO morphology is revealed by TEM. As can be seen in Figure 3c the transparent graphene sheets are randomly folded due to defective structure formed upon electrochemical reduction. Figure 3d shows the HRTEM of ErGO which consists of 8-9 layers of graphene sheets. The interlayer distance of the sheets is about 0.38 nm which corresponds to the (002) plane of ErGO.

Effect of GO loading on ORR performance

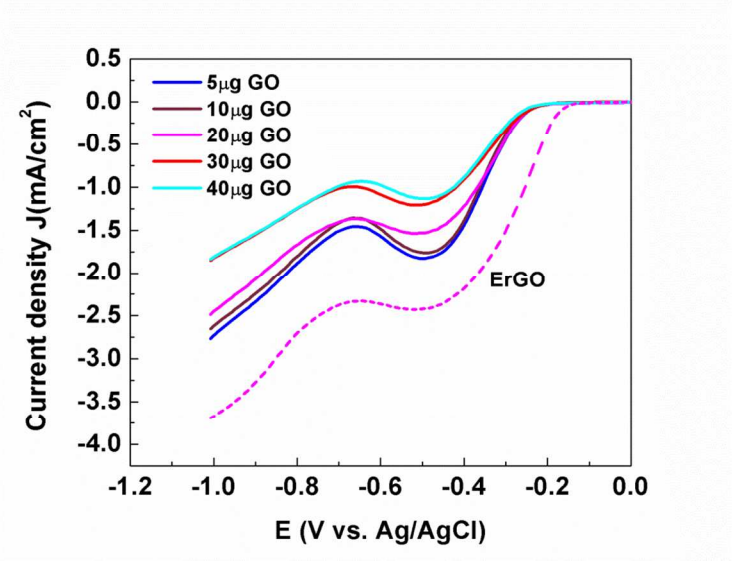

Fig. 4: Linear-sweep voltammetry curves of GO with various mass loadings and ErGO in O_2 saturated 0.1 M KOH electrolyte at a scan rate of 10 mV/s and a rotation rate of 1600 rpm.

To gain an insight into the role of the GO catalyst loading during the ORR electrochemical process we investigated its electrocatalytic performance as a function of mass loading. We carried out the linear sweep voltammetric (LSV) measurements on a rotating disk electrode (RDE) with GO loadings varying from 5 μg to 40 μg on a GCE in an O_2 saturated 0.1 M KOH electrolyte solution. All five loadings showed a substantial reduction process in the presence of oxygen. As shown in Figure 4 the onset and peak potentials of ORR did not show any substantial change with mass loading, however a systematic decrease on current density was observed consistent with the insulating nature of GO. The typical two-step pathway was observed for the GO electrode with onset potentials at around -0.28 V and -0.65 V, indicating a successive two-electron reaction pathway.

ORR performance

The reduction of oxygen in alkaline solutions can proceed by two major pathways: A direct four electron pathway and a two electron 'peroxide' pathway according to equations (2) and (3).[47, 48]

$$O_2 + 2H_2O + 4e^- \longrightarrow 4OH^- \qquad (2)$$

$$O_2 + H_2O + 2e^- \longrightarrow HO_2^- + OH^- \qquad (3)$$

Alternatively the peroxide (HO_2^-) can be further reduced according to a further $2e^-$ reduction (4)

$$HO_2^- + H_2O + 2e^- \rightarrow 3OH^- \qquad (4)$$

Or through a disproportionation reaction (5)

$$HO_2^- \rightarrow \frac{1}{2}O_2 + OH^- \qquad (5)$$

It is worth noting that summation of the two sequential two electron reductions (involving peroxide) (3 and 4) leads to the respective 4 electron reduction.

The electrocatalytic activities of the GO/GCE, ErGO/GCE, and NrGO/GCE electrodes were evaluated by CV and RDE voltammetries. A catalyst with a higher electrocatalytic activity toward the ORR will demonstrate an earlier onset potential and a higher peak current. Accordingly, its RDE voltammograms should also show a sooner current drop with a positively shifted onset potential and a higher steady-state current.

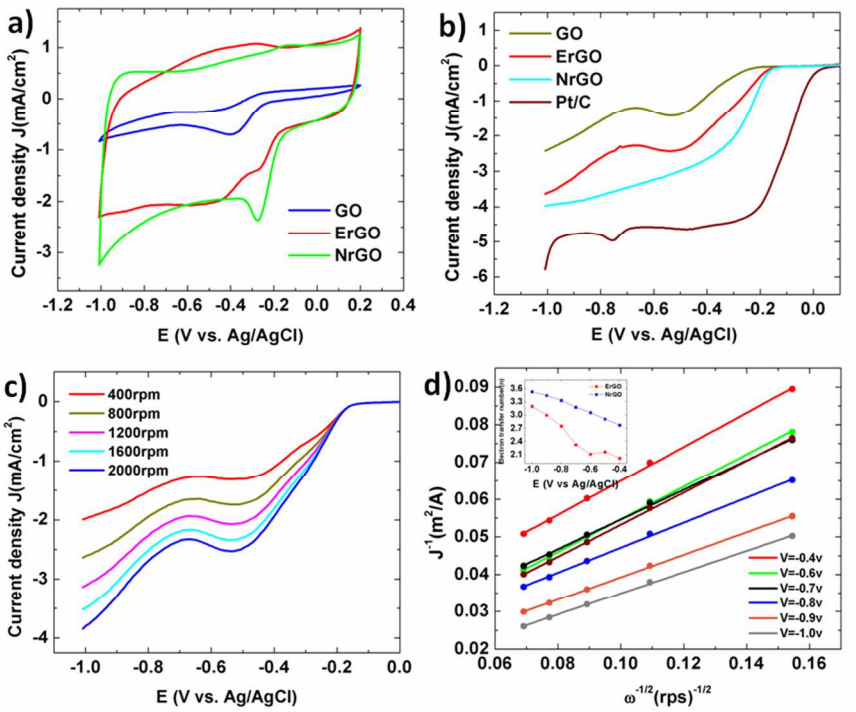

Fig. 5: (a) CV curves of oxygen reduction on the GO, ErGO, NrGO electrodes in an O_2 saturated 0.1 M KOH solution at a scan rate of 100 mV/sec (b) RDE curves for oxygen reduction on the GO, ErGO and Pt/C electrodes in an O_2 saturated 0.1 M KOH solution at a scan rate of 10 mV/s (c) Rotating disk voltammograms of ErGO in O_2 saturated 0.1 M KOH at different rotation rates. (d) Corresponding Koutecky–Levich lot (I−1 vs. ω−0.5) at different potentials and the inset shows the n numbers of ErGO and NrGO.

The cyclic voltammograms (CVs) of GO, ErGO and NrGO in an aqueous O_2 saturated 0.1 M KOH solution is shown in Figure (5a). As can be seen, the onset

potential of ORR for the GO electrode subjected to 22 reducing CVs is at -0.18 V (versus AgCl) with the cathodic reduction peak around -0.40 V (versus Ag/AgCl). Upon electrochemical reduction of GO both the onset potential and the ORR reduction peak potential shifted positively to -0.11 V and -0.26 V respectively, accompanied by a concomitant increase in the peak current density (Figure 5a). These results clearly demonstrated a significant enhancement in the ORR electrocatalytic activity for the ErGO in respect to the graphene oxide electrode. Compared with GO, the ErGO shows dramatically increased capacitance similar to NrGO, this is mainly related to increased conductivity of the material. The change in shape of the CV curves demonstrates the increase of non-Faradaic currents induced by the increase in effective surface area of electrically conductive graphene that is generated by reduction of GO.

To further investigate the ORR performance, we carried out the linear sweep voltammetric (LSV) measurements on a rotating disk electrode. As shown in Figure 5b, the ORR at the GO electrode commenced around -0.18 V (onset potential), whereas the ORR onset potential at the ErGO electrode subjected to 22 reducing CVs significantly shifted positively to -0.11 V with the limiting diffusion current at -1 V being about 1.7 times higher than that of the GO electrode. For the GO and ErGO, a clear reduction pre-wave is observed at low overpotentials, followed by a second reduction wave starting around -0.7 V, this being indicative of a prevalent $2e^-$ reduction path.[56,57] The absence of the peak in the LSV of NrGO at -0.7 V (Figure 5b) suggests that NrGO has a more efficient oxygen reduction due to the presence of nitrogen related electrocatalytic active sites for oxygen reduction.

Figure S4 presents the as measured LSVs of 20 µg of GO coated on GCE before and after electrochemical reduction. In the same graph we present the LSV of ErGO after subtracting the background signal. The LSV background signal was obtained in N_2 saturated 0.1 M KOH solution. The significantly more positive onset potential of ErGO (-0.18 V for GO vs -0.11V for ErGO) and the higher current clearly demonstrate that the improved electrocatalytic activity after electrochemical reduction is not due to the background signal or due a difference in the mass loading.

Rotating disk electrode (RDE) is used to reveal the ORR kinetics of ErGO in O_2 saturated 0.1 M KOH solution. As shown in the Figure 5c as rotation speed increases the oxygen reduction current also increases. Inset of figure 5d shows the electron transfer number (n) for ErGO and NrGO. In the case of ErGO electron transfer number (n) was calculated to be 2 – 3.3 in the voltage range -0.4 V to -1.0 V from the slopes of Koutecky Levich plots. At low overpotentials (<−0.7 V) the value of n is close to two and the reduction of O_2 produces HO_2^-. At more negative potentials the n value gradually increases, which indicates that the peroxide formed reduces further to OH^- in this potential range. In the case of the NrGO, the electron transfer numbers (n) were substantially larger ranging from 2.7 to 3.5 in the voltage range -0.4 V to -1.0 V, which suggest that the NrGO is more electro active when compared to ErGO. The absence of the peak in the LSV of NrGO at -0.7 V (Figure 5b) suggests that NrGO has a high number of electrocatalytic active sites for oxygen reduction. Although both catalysts operate under combined $4e^-$ and $2e^-$ ORR processes, ErGO follows a more predominant $2e^-$ e pathway. (Figure 5b)

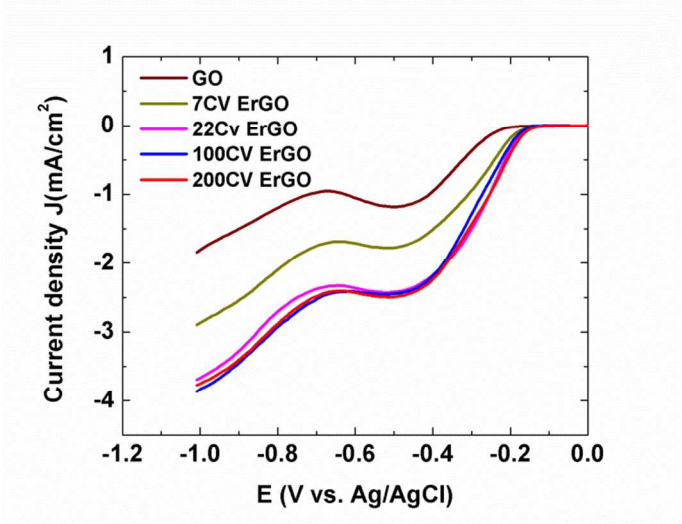

Fig. 6: Shows the rotating disk voltammograms in O_2 saturated 0.1 M KOH at a scan rate of 10 mV/s and 1600 rpm of GO subjected to different reduction cycles.

Figure 6 shows that reduction of GO for more than 22 cycles didn't show any substantial improvement in ORR performance.

Various surface functional groups, such as hydroxyl, carboxylic, carbonyl are present on the graphene surfaces. A long standing question is which types of functional groups are responsible for electrocatalysis of oxygen reduction.[49] Quinone functional groups have been postulated as catalytic sites for $2e^-$ ORR on carbon materials, with means that the reduction of oxygen stops at the peroxide stage. However for ErGO the presence of additional oxygen groups may catalyse the further reduction of hydrogen peroxide (HO_2^-) at more negative potentials as exemplified by the increased n numbers. Similar increment in the n numbers was observed between a polished and an oxidised GC electrode where the reduction current of the anodised GC exceeded significantly the limiting current of the $2e^-$ process.[50] It should be noted that the presence of cation species such as Na^+ accrued from the reduction process may have an influence on the electron transfer process and play a role on the ORR.

Electrochemically Active Surface Area

In addition we have estimated the electrochemical active surface area (EASA) of GO and ErGO electrodes by the following equation (6).[51, 52]

$$\text{EASA} = \frac{C_{dl}}{C_s} \qquad (6)$$

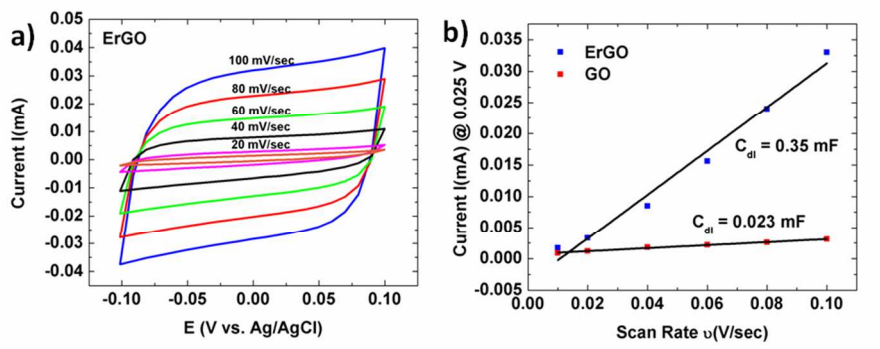

Fig.7: (a) Cyclic voltammograms of ErGO in the potential range of -0.1 V to +0.1 V vs. Ag/AgCl (non-Faradaic region) at scan rates of 100 mV/sec, 80 mV/sec, 60 mV/sec, 40 mV/sec, 20 mV/sec and 10 mV/sec in N_2 saturated 0.1 M KOH solution. (b) The cathodic charging current measured at 0.025V vs. Ag/AgCl as a function of scan rate for ErGO and GO.

Where C_{dl} is electrochemical double-layer capacitance of the catalytic surface, and C_s (specific capacitance) is the double layer capacitance of an atomically smooth planar surface of the material per unit area under same electrolyte conditions. To measure C_{dl}, a potential range in which no apparent Faradaic processes occur was chosen. The C_{dl} was determined by measuring the non-Faradaic capacitive current associated with double-layer charging from the scan-rate dependence of cyclic voltammograms (CVs) as shown in Figure (3). The double layer charging current (i_c) is equal to the product of scan rate (ν) and double layer capacitance (C_{dl}) as given by equation (7).[51-54]

$$i_c = \nu \cdot C_{dl} \qquad (7)$$

Thus a plot of i_c versus ν gives a straight line with a slope equal to the C_{dl} as shown in Figure (3b). The estimated C_{dl} values of GO and ErGO are 0.023 mF and 0.35 mF. Specific capacitances for carbon electrode materials have been measured in alkaline and acidic solutions and typical values reported range between $\mathbf{C_s}$ = **0.005−0.055** mF cm^{-2} in alkaline and acid solutions.[55] We use specific capacitances of C_s = **0.020** mF cm^{-2} for both GO and ErGO as representative reported values. The C_{dl} and EASA values of each material are shown are shown in Table S1. The estimated EASA of GO and ErGO are 1.05 cm^2 and 15.9 cm^2. The EASA of ErGO is 15 times higher than the GO.

Methanol poisoning

To examine the possible crossover effect in the presence of other fuel molecules (e.g., methanol) linear sweep voltammetric responses for ORR at the ErGO and Pt/C electrodes were obtained. As shown in Figure 7a, for the commercial Pt/C catalyst, a sharp increase in the onset ORR potential and a net positive current were observed in the presence of 2.5 M methanol concentration. These changes indicate that the methanol-oxidation reaction (MOR), rather than the ORR, was the preferred reaction

on the Pt/C electrode. In contrast, the corresponding onset potential and overall performance of the ErGO electrode remained almost unchanged by the presence of MeOH (Figure 7b). The results unambiguously show that the ErGO has much better methanol tolerance than the commercial Pt/C catalyst.

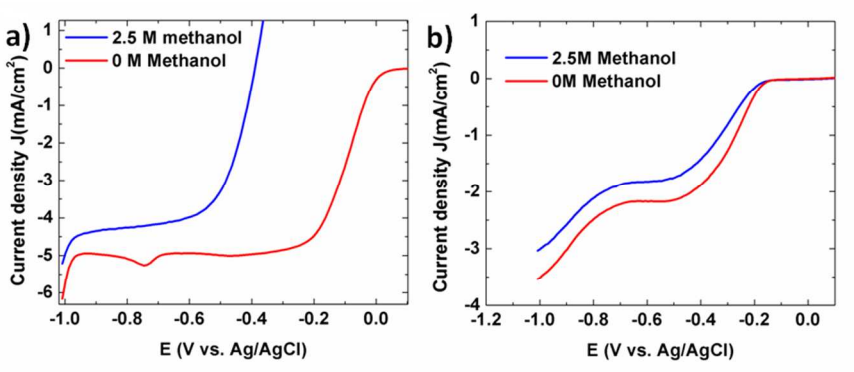

Fig. 8: (a) Polarization curves for ORR on commercial Pt/C catalyst in an O_2-saturated 0.1 M KOH electrolyte containing 2.5 M methanol at a rotation rate of 1600 rpm and scan rate of 10 mV/s. (b) Polarization curves for ORR on ErGO electrode in an O_2 saturated 0.1 M KOH electrolyte containing 2.5 M methanol at a rotation rate of 1600 rpm and scan rate of 10 mV/s.

Impedance studies

The EIS technique has been used to probe the interfacial processes of ORR electrode reactions. Figure 8 displays EIS spectra in the form of Nyquist plot, for GO and ErGO electrodes at a bias of -0.165 V respectively. ErGO shows a small semicircle at intermediate and low frequency region whereas the GO shows a tremendous large arc, suggesting a very slow or negligible reaction rate of ORR and extremely large charge transfer resistance compared to ErGO. It is clear that the impedance values measured from the GO electrode are higher than those of the ErGO illustrating the resistive and conductive character of GO and ErGO respectively.

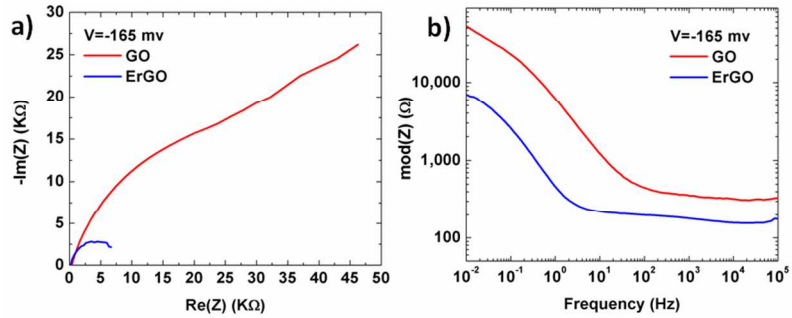

Fig. 9: (a) Nyquist plots and (b) Bode plots of GO and ErGO obtained at a bias of -0.165 V over the frequency range from 100 kHz to 10 mHz.

Conclusions

We have shown that nitrogen free electrochemically reduced graphene oxide (ErGO) displays significantly enhanced catalytic activity toward oxygen reduction reaction

in alkaline solutions compared to the initial unreduced GO electrode. However its ORR activity is inferior to that of nitrogenated graphene oxide (NrGO) prepared by hydrothermal treatment. The electrochemical partial reduction of GO was confirmed by X-ray diffraction and X-ray photoelectron spectroscopy. Electrochemical impedance spectroscopy (EIS) verified the enhanced electron transfer ability of the electrochemically reduced graphene oxide (ErGO) compared to GO. Kinetic studies revealed that although both ErGO and NrGO catalysts operate under combined $4e^-$ and $2e^-$ ORR processes, ErGO follows a more predominant $2e^-$ pathway. This ORR pathway in ErGO has been linked to the presence of quinone functional groups, which favour the $2e^-$ ORR process.

Acknowledgements

This work was financially supported by VCRS studentship from the University of Ulster. XPS was performed at the National EPSRC XPS User's Service (NEXUS) at Newcastle University, an EPSRC Mid-Range Facility.

References

[1]*School of Engineering, Engineering Research Institute, University of Ulster, Newtownabbey, BT37 0QB, UK. Corresponding author E -mail: p.papakonstantinou@ulster.ac.uk*
[2]*School of Mechanical and Systems Engineering, University of Newcastle, Stephenson Building, Newcastle upon Tyne NE1 7RU, UK.*
[3]*School of the Built and Environment, University of Ulster, Newtownabbey, BT37 0QB, UK.*

1 F. Cheng and J. Chen, *Chem. Soc. Rev.,* 2012, **41,** 2172.
2 L. Qu, Y. Liu, J. Baek and L. Dai, *ACS Nano,* 2010, **4,** 1321.
3 H. Wang, T. Maiyalagan and X. Wang, *ACS Catalysis,* 2012, **2,** 781.
4 Z. Yang, Z. Yao, G. Li, G. Fang, H. Nie, Z. Liu, X. Zhou, X. Chen and S. Huang, *ACS Nano,* 2012, **6,** 205.
5 Z. Liu, F. Peng, H. Wang, H. Yu, W. Zheng and J. Yang, *Angewandte Chemie International Edition,* 2011, **50,** 3257.
6 C. Zhu and S. Dong, *Nanoscale,* 2013, **5,** 1753.
7 Z. Sheng, H. Gao, W. Bao, F. Wang and X. Xia, *J. Mater. Chem.,* 2012, **22,** 390.
8 N. Daems, X. Sheng, I. F. J. Vankelecom and P. P. Pescarmona, *J.Mater.Chem.A,* 2014, **2,** 4085.
9 X. Kong, C. Chen and Q. Chen, *Chem. Soc. Rev.,* 2014, **43,** 2841.
10 J. Park, Y. J. Jang, Y. J. Kim, M. Song, S. Yoon, D. H. Kim and S. Kim, *Phys. Chem. Chem. Phys.,* 2014, **16,** 103.
11 R. Li, Z. Wei, X. Gou and W. Xu, *RSC Adv.,* 2013, **3,** 9978.
12 Z. Yao, H. Nie, Z. Yang, X. Zhou, Z. Liu and S. Huang, *Chem.Commun.,* 2012, **48,** 1027.
13 S. Wang, L. Zhang, Z. Xia, A. Roy, D. W. Chang, J. Baek and L. Dai, *Angewandte Chemie International Edition,* 2012, **51,** 4209.
14 J. Liang, Y. Jiao, M. Jaroniec and S. Z. Qiao, *Angewandte Chemie International Edition,* 2012, **51,** 11496.
15 Y. Zheng, Y. Jiao, L. Ge, M. Jaroniec and S. Z. Qiao, *Angewandte Chemie International Edition,* 2013, **52,** 3110.
16 L. Zhang, J. Niu, L. Dai and Z. Xia, *Langmuir,* 2012, **28,** 7542.
17 L. Zhang and Z. Xia, *The Journal of Physical Chemistry C,* 2011, **115,** 11170.
18 A. Ganguly, S. Sharma, P. Papakonstantinou and J. Hamilton, *J. Phys. Chem. C,* 2011, **115,** 17009.
19 D. Li, M. B. Muller, S. Gilje, R. B. Kaner and G. G. Wallace, *Nat Nano,* 2008, **3,** 101.
20 H. Shin, K. K. Kim, A. Benayad, S. Yoon, H. K. Park, I. Jung, M. H. Jin, H. Jeong, J. M. Kim, J. Choi and Y. H. Lee, *Advanced Functional Materials,* 2009, **19,** 1987.
21 A. Ambrosi, C. K. Chua, A. Bonanni and M. Pumera, *Chemistry of Materials,* 2012, **24,** 2292.
22 D. Long, W. Li, L. Ling, J. Miyawaki, I. Mochida and S. Yoon, *Langmuir,* 2010, **26,** 16096.

23 Y. Su, Y. Zhang, X. Zhuang, S. Li, D. Wu, F. Zhang and X. Feng, *Carbon,* 2013, **62,** 296.
24 A. Ambrosi and M. Pumera, *Chemistry A European Journal,* 2013, **19,** 4748.
25 X. Peng, X. Liu, D. Diamond and K. T. Lau, *Carbon,* 2011, **49,** 3488.
26 A. J. Haque, H. Park, D. Sung, S. Jon, S. Choi and K. Kim, *Anal. Chem.,* 2012, **84,** 1871.
27 Y. Cao, M. Zhu, P. Li, R. Zhang, X. Li, Q. Gong, K. Wang, M. Zhong, D. Wu, F. Lin and H. Zhu, *Phys.Chem.Chem.Phys.,* 2013, **15,** 19550.
28 X. Xu, D. Huang, K. Cao, M. Wang, S. M. Zakeeruddin and M. Grätzel, *Sci. Rep.,* 2013, **3,** 1489.
29 D. Huang, B. Zhang, Y. Zhang, F. Zhan, X. Xu, Y. Shen and M. Wang, *J. Mater. Chem. A,* 2013, **1,** 1415.
30 J. Yang and S. Gunasekaran, *Carbon,* 2013, **51,** 36.
31 X. Liu, X. Qi, Z. Zhang, L. Ren, G. Hao, Y. Liu, Y. Wang, K. Huang, X. Wei, J. Li, Z. Huang and J. Zhong, *RSC Adv.,* 2014, **4,** 13673.
32 M. A. Raj and S. A. John, *The Journal of Physical Chemistry C,* 2013, **117,** 4326.
33 Y. Shao, J. Wang, M. Engelhard, C. Wang and Y. Lin, *J. Mater. Chem.,* 2010, **20,** 743.
34 L. Yang, D. Liu, J. Huang and T. You, *Sensors Actuators B: Chem.,* 2014, **193,** 166.
35 K. Sheng, Y. Sun, C. Li, W. Yuan and G. Shi, *Sci. Rep.,* 2012, **2,** 247.
36 X. Peng, X. Liu, D. Diamond and K. T. Lau, *Carbon,* 2011, **49,** 3488.
37 Y. Cao, M. Zhu, P. Li, R. Zhang, X. Li, Q. Gong, K. Wang, M. Zhong, D. Wu, F. Lin and H. Zhu, *Phys.Chem.Chem.Phys.,* 2013, **15,** 19550.
38 M. A. Raj and S. A. John, *J. Phys. Chem. C,* 2013, **117,** 4326.
39 V. Mani, B. Devadas and S. Chen, *Biosensors and Bioelectronics,* 2013, **41,** 309.
40 J. Ping, Y. Wang, Y. Ying and J. Wu, *Anal. Chem.,* 2012, **84,** 3473.
41 C. Zhu, S. Guo, Y. Fang, L. Han, E. Wang and S. Dong, *Nano Research,* 2011, **4,** 648.
42 P. Papakanstantinou, S. Surbhi, S.K. Bikkarolla, A.Ganguly, D. James, *WIPO PATENTS,* 2012, (WO 2012/114108 A1) .
43 S. Stankovich, D. A. Dikin, R. D. Piner, K. A. Kohlhaas, A. Kleinhammes, Y. Jia, Y. Wu, S. T. Nguyen and R. S. Ruoff, *Carbon,* 2007, **45,** 1558.
44 C. Chen, Q. Zhang, M. Yang, C. Huang, Y. Yang and M. Wang, *Carbon,* 2012, **50,** 3572.
45 H. Zhang, T. Kuila, N. H. Kim, D. S. Yu and J. H. Lee, *Carbon,* 2014, **69,** 66.
46 K. N. Kudin, B. Ozbas, H. C. Schniepp, R. K. Prud'homme, I. A. Aksay and R. Car, *Nano Letters,* 2008, **8,** 36.
47 B. E. Conway, *Plenum Press, New York,* 1983, **7,** 301.
48 E. Yeager, *Electrochim. Acta,* 1984, **29,** 1527.
49 B. Sljukic, C. E. Banks and R. G. Compton, *Journal of the Iranian Chemical Society,* 2005, **2,** 1.
50 K. Vaik, D. J. Schiffrin and K. Tammeveski, *Electrochemistry Communications,* 2004, **6,** 1.
51 S. Trasatti, O. A. Petrii, *Pure Appl. Chem.,* 1991, **63,** 711.
52 R. Boggio, A. Carugati and S. Trasatti, *J. Appl. Electrochem.,* 1987, **17,** 828.
53 C. C. L. McCrory, S. Jung, J. C. Peters and T. F. Jaramillo, *J. Am. Chem. Soc.,* 2013, **135,** 16977.
54 J. D. Benck, Z. Chen, L. Y. Kuritzky, A. J. Forman and T. F. Jaramillo, *ACS Catal.,* 2012, **2,** 1916.
55 (a) T. A. Centeno and F. Stoeckli, *J. Power Sources,* 2006, **154,** 314; (b) D. Qu, *J. Power Sources*, 2002, **109**, 403; (c) R. Signorelli, D. C. Ku, J. G. Kassakian and J. E. Schindall, 2009, *Proceedings of the IEEE*, 2009, **97**, 1837(d). M. D. Stoller, C. W. Magnuson, Y. Zhu, S. Murali, J. W. Suk, R. Piner and R. S. Ruoff, *Energy Environ. Sci.*, 2011, **4**, 4685.
56 C. Song and J. Zhang, Electrocatalytic Oxygen Reduction Reaction, ed., Springer London, 2008, 89.
57 I. Kruusenberg, J. Leis, M. Arulepp and K. Tammeveski, *Journal of Solid State Electrochemistry*, 2010, **14**, 1269.